

Phase stabilization principle and precipitate-host lattice influences for Al–Mg–Si–Cu alloy precipitates

F. J. H. Ehlers¹, S. Wenner¹, S. J. Andersen², C. D. Marioara², W. Lefebvre³, C. B.

Boothroyd⁴ and R. Holmestad^{1*}

¹Department of Physics, Norwegian University of Science and Technology, NTNU,

7491 Trondheim, Norway

²SINTEF, Materials and Chemistry, 7465 Trondheim, Norway

³Groupe de Physique des Matériaux, Université de Rouen, 76801 St. Etienne du

Rouvray, Cedex, France

⁴Ernst Ruska-Centre for Microscopy and Spectroscopy with Electrons (ER-C) and Peter

Grünberg Institute (PGI), Forschungszentrum Jülich, D-52425 Jülich, Germany

Abstract

In this work, we seek to elucidate a common stabilization principle for the metastable and equilibrium phases of the Al–Mg–Si–Cu alloy system, through combined experimental and theoretical studies. We examine the structurally known well-ordered Al–Mg–Si–Cu alloy metastable precipitates along with experimentally observed disordered phases, using high angle annular dark field scanning transmission electron microscopy. A small set of local geometries is found to fully explain all structures. Density functional theory based calculations have been carried out on a larger set of structures, all fully constructed by the same local geometries. The results reveal that experimentally reported and hypothetical Cu-free phases from the set are practically indistinguishable with regard to formation enthalpy and composition. This strongly supports a connection of the geometries with a bulk phase stabilization principle. We relate our findings to the Si network substructure commonly observed in all Mg–Al–

Si(-Cu) metastable precipitates, showing how this structure can be regarded as a direct consequence of the local geometries. Further, our proposed phase stabilization principle clearly rests on the importance of metal-Si interactions. Close links to the Al-Mg-Si precipitation sequence are proposed.

*) Corresponding author: Tel.: +47 7359 3880; fax: +47 7359 7710; email:

randi.holmestad@ntnu.no

Keywords: Aluminum alloys; Precipitation; Phase stabilization principles; Transmission electron microscopy; Density functional theory

1. Introduction

Age hardenable Al-Mg-Si(-Cu) (6xxx) alloys are widely used by the industry due to desirable properties such as high strength-to-weight ratio, good formability and high corrosion resistance. Over the last decade in particular, developments in transmission electron microscopy (TEM) techniques have led to structure identification of most of the metastable precipitates responsible for alloy hardening in this system [1-8]. For Al-Mg-Si, the generally accepted alloy precipitation sequence reads [9,10]:



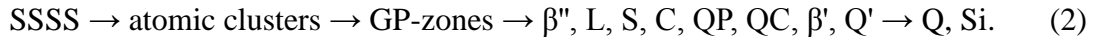
All the metastable phases (pre- β'' to β') in (1) grow as needles/rods/laths along $\langle 001 \rangle_{\text{Al}}$ directions in the face-centered cubic (fcc) Al host lattice, from an original quenched-in alloying element supersaturated solid solution (SSSS).

The detailed knowledge acquired on the individual precipitate structures in principle permits atomistic level considerations on precipitate nucleation and growth [11-15]. It

is well established that metastable hardening phases emerge from the SSSS in close interplay with the surrounding fcc Al. Also, these phases are generally believed to bear some clear structural and chemical resemblance to the equilibrium phases of the system. However, in the case of (1), such links have remained elusive, with the main hardening phase β'' providing the key example [2, 16].

Conversely, a uniting feature among the metastable Al–Mg–Si phases has also been noted. Cayron *et al.* [17] reported the presence of a common substructure, more recently shown by Andersen *et al.* [18] to be composed of Si atoms. When viewed along the precipitate main growth (needle/rod/lath) direction, these atoms create a structure with projected hexagonal symmetry [4, 19]. This 'Si network' regularity is practically perfect for all phases but β'' , where the network is visibly distorted [2]. Along the network c -axis, i.e. out of the projected hexagonal plane, most precipitates are fully coherent ($c = 4.05 \text{ \AA}$ [4]) with fcc Al. The exception is the β' phase, which is fully coincidence site [20] coherent, $c = 4.05 \text{ \AA} \times 3$ [5]. The Si column separation (network a -axis) is always $\approx 4.0 \text{ \AA}$ [4, 19].

The Si network definition makes room for a *class* of such substructures. Adding to this inherent ambiguity, the network has not been observed in either of the equilibrium phases of (1), β and Si. Compelling arguments for a connection with a phase construction principle have so far been lacking. For Al–Mg–Si–Cu, this aim may be more feasible, as clarified below. Upon introduction of Cu to Al–Mg–Si, the precipitate sequence (1) is changed into [8]:



Compared to (1), all additional phases in (2) are Cu-bearing. All metastable phases in (2) contain the Si network and grow primarily as needles/rods/laths along the network c -axis, $\parallel \langle 001 \rangle_{\text{Al}}$. In this respect, (1) and (2) appear identical. A series of observations serve to show, however, that the Al–Mg–Si–Cu phases are structurally more closely linked:

- (i) The equilibrium phase Q in (2) contains the Si network [11].
- (ii) All well-ordered metastable Cu-bearing phases (C and Q') in (2) are fully coherent with **fcc** Al along their main growth direction [7].
- (iii) For all Cu-bearing phases in (2), the number of atoms outside the network is seemingly always twice the number of network atoms [8]. We shall refer to this precipitate atom subset as 'non-network atoms' below. In (1), only U2 and B' satisfy this criterion.
- (iv) Cu appears to prefer the same local geometry for all Cu-bearing phases in (2) [8, 21].
- (v) Of the disordered phases in (2), the important hardening phase L generally contains local regions of the well-ordered phases C and Q' [8, 21].

We suspect from points (i) – (v), that atomistic studies of (2) provide a better opportunity to elucidate the Si network significance. Various theoretical studies [7, 11, 22] have already examined the phases C, Q', and Q. However, we are not aware of any attempts to clarify the structural links among the phases in (2).

In this work, we perform (Sec. 3) an atomistic analysis of the Al–Mg–Si–Cu metastable phases C, Q', and L, using high angle annular dark field scanning TEM (HAADF-STEM). From these investigations, we identify a series of local geometries intimately connected with the Si network formation in these structures. We then propose that all metastable Cu containing phases in (2), regardless of long range order, can be fully deconstructed into these local geometries. In Sec. 5, we list a series of experimentally reported as well as hypothetical phases, all constructed according to the proposed principle. Phase stabilities are addressed through density functional theory (DFT) based studies. In all cases, competitive formation energies are predicted. Finally, we deconstruct a selected L precipitate into the local geometries as a first support of the validity of the proposed construction principle for this phase. Sec. 6 summarizes our findings. For preliminary work into these issues, see [23].

2. Experimental details

For the experimental investigations of this work, discussed in Sec. 3, three different alloys were selected. The C phase studies involved an alloy with composition Al–1.00Mg–0.62Si–0.14Cu–0.03Ag–0.10Fe–0.27Mn (at. %). As discussed in [7], the presence of weak amounts of Ag had no notable influence on the precipitate structures observed. The alloy was subjected to homogenization for 4 h at 530 °C, followed by extrusion, solutionizing for 30 min at 530 °C, 4 h storage at room temperature (RT), 12 h aging at 155 °C, and finally, overaging for 3 weeks at 200 °C. This heat treatment does not necessarily optimize the presence of C, which is seemingly always a rare precipitate in its pure state [7]. For the studies of Q', an alloy with composition Al–0.68Mg–0.93Si–0.19Cu–0.10Fe–0.27Mn (at. %) was chosen, while the alloy selected

for the L phase investigations had composition Al–1.00Mg–0.62Si–0.17Cu–0.10Fe–0.27Mn (at. %). Here, the alloy compositions were specifically chosen to optimize the phases of interest. Both alloys were subjected to the same heat treatment, differing from the one described for the C phase for the last step only: the overaging in this case lasted only 1 week.

HAADF-STEM specimens were prepared by electropolishing using a Tenupol 3 machine. The electrolyte consisted of 1/3 HNO₃ in methanol and was kept at a temperature between –20 and –35 °C during polishing. A probe spherical aberration (Cs) corrected FEI Titan 80-300ST TEM/STEM, operating at 300 kV, with a 40-50 mrad inner collector angle and nominal 0.8 Å probe size, was used for the C phase HAADF-STEM imaging. Both the Q' and the L precipitates were imaged in probe Cs-corrected HAADF-STEM mode. In these cases, the microscope used was a JEOL ARM 200F, operating at 200 kV, with a 40 mrad inner collector angle and a 1 Å probe size.

3. Geometrical units of the Al–Mg–Si–Cu metastable phases

3.1. Experimental background: C and Q' phases

The well-ordered (unit cell hosting) metastable phases so far observed for the Al–Mg–Si–Cu alloy system are well characterized experimentally. Figs. 1a and 1b display Cs-corrected HAADF-STEM images of the Cu-bearing subset, C and Q', respectively. The C phase structure and composition was recently determined by Torsæter *et al.* [7]. Q' is isostructural to the equilibrium phase Q in (2) [11, 24], the structure of which was clarified decades ago by Arnberg and Aurivillius [25]. Fig. 1c shows an example of the disordered L precipitate [8, 21], one of the main hardening

phases of Al–Mg–Si–Cu. All images in Fig. 1, recorded at the $\langle 001 \rangle_{\text{Al}}$ zone, show cross-sections of precipitates embedded in the aluminum. In each case, the main growth direction of these plate/lath shaped phases [8] is pointing out of the paper. Since the particles cut through the entire TEM foil, there is no overlap with the aluminum matrix in this direction. To reduce noise, the images were low-pass Fourier filtered using a circular mask excluding spacings shorter than 1.7 Å.

Each bright spot for the images in Fig. 1 represents an atomic column in the viewing direction. The intensity in the HAADF-STEM image varies approximately as the square of the atomic number, Z^2 [26]. Hence, Cu-rich columns clearly stand out relative to any other columns. The second strongest scattering atom present is Si. The ordering of these atoms into the network, discussed in Sec. 1, is also directly discernible. Both of these features have been highlighted in Figs. 1a and 1b over a part of the cross-section. We note that the Cu column arrangement in C and Q' reveals the underlying unit cell of each ordered phase. When turning to the disordered L phase in Fig. 1c, it is evident from the observed Cu arrangement here that C and Q' are present locally within the precipitate. Other regions are visibly Cu-poor. From the network overlay for the three phases in Figs. 1a - 1c, we deduce network a -axes along $\langle 100 \rangle_{\text{Al}}$ for C and L. By comparison, for Q'/Q, this axis is mainly along $\langle 510 \rangle_{\text{Al}}$ [8]. In particular, this means that when Q' is present in L, the network is rotated by $\approx 11^\circ$ about its c -axis, to comply with the different network orientation of this phase. In its pure state, Q' possesses at least one coherent interface with fcc Al, as directly observed in Fig. 1b (top left). For a discussion into the precipitate-host lattice interface characteristics for the reoriented Q' phase, we refer to Sec. 5.3.

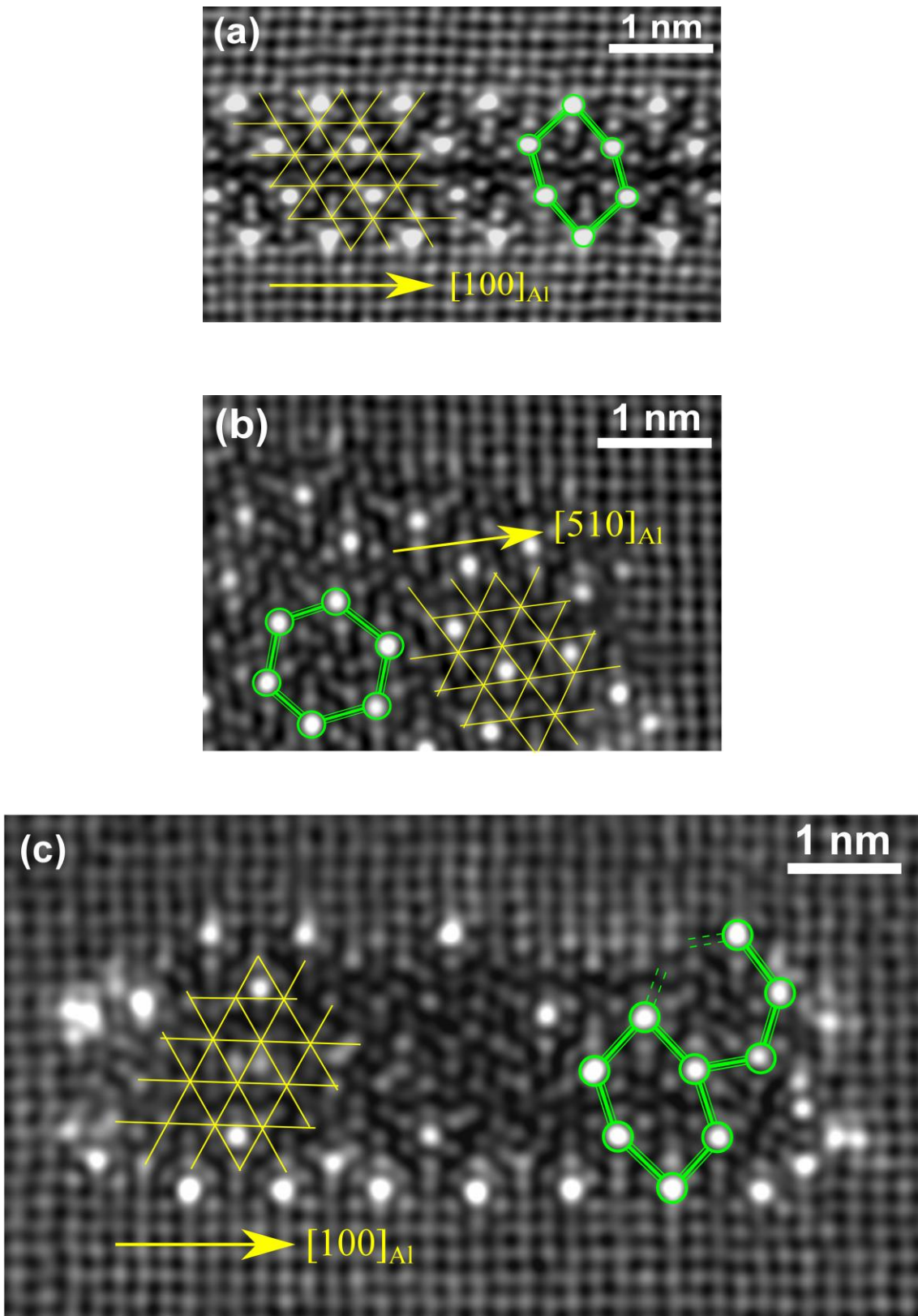


Fig. 1 HAADF-STEM images ($\langle 001 \rangle_{Al}$ zone) of cross-sections of selected metastable

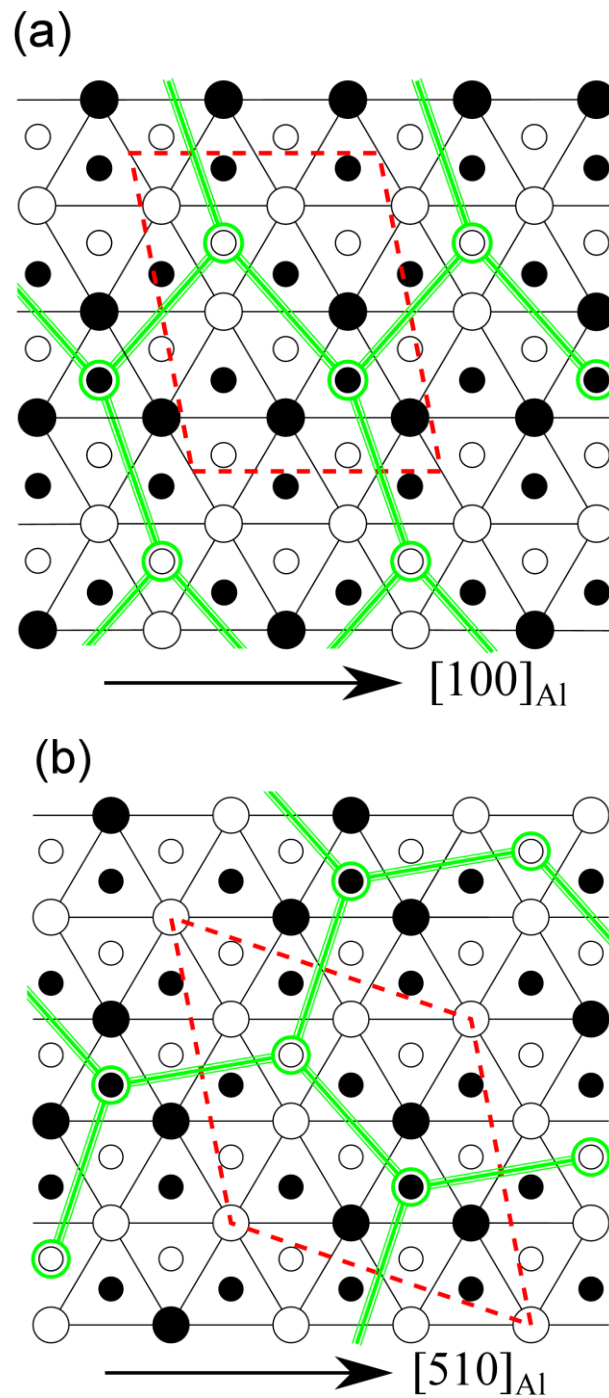
precipitates in the Al–Mg–Si–Cu system. The precipitates have their main growth direction out of the plane. In each Fourier filtered image, the bright spots correspond to projected columns of atoms. The strongest intensities denote high Cu contents. Local Cu ordering has been highlighted by broad green lines. The hexagonally arranged Si columns (network) represent the second strongest scattered intensities. These columns reside at the intersection of the overlaid thin yellow lines. The precipitates are (a): C phase, (b): Q' phase, and (c): a disordered L precipitate. Regions of C and Q' (as well as nearly Cu free regions) are directly visible in the last precipitate (c)

The images of Fig. 1 visually highlight the close structural link between L and C, Q', with the seamless coupling of Cu-rich and Cu-poor regions in the disordered phase managed through the Si network. Even in the Cu-poor regions for the L precipitate, each projected network triangle is enclosing one non-network atom, indicating that point (iii) of Sec. 1 is fulfilled. A few local violations of point (iv) in Sec. 1 are observed. Certain isolated network atom columns near the interface with the host lattice in Fig. 1c have much higher intensity, hence containing Cu (see also [27]). Nevertheless, the above considerations arguably provide an indication that any local structural connections between the ordered phases C and Q' may be extended to L.

3.2. Decomposing the Si network into geometrical units

Figs. 2a and 2b display schematically the C and Q' phases, in the same orientation as chosen in Figs. 1a and 1b, respectively. All Si columns are connected with lines, highlighting the projected network triangles each enclosing a non-network column. Only two different atom heights are allowed in the viewing direction (network c -axis), given the full coherency of both phases with Al along this $\langle 001 \rangle_{\text{Al}}$ direction.

With the height of white atoms generally defined here as 0 Å, black atoms are translated by 2.025 Å in the viewing direction. The general discussion includes gray atoms at (undecided) heights of either 0 Å or 2.025 Å, see Fig. 2c. The figures ignore structural relaxation of the non-network substructure, placing each atom here at the center of its associated network triangle.



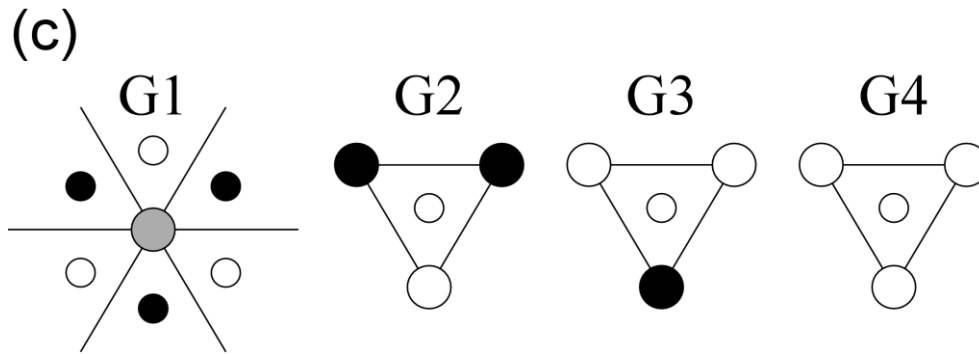


Fig. 2 Schematic representation (same orientation as in Figs. 1a and 1b) of (a) the C phase and (b) the Q' phase. Relative atom heights are highlighted by the color of the spheres: white = 0 Å; black = 2.025 Å (spacing of fcc Al planes along $[001]_{\text{Al}}$); gray = either. Si network atoms are characterized by bigger spheres, and connected with full lines. For simplicity, all remaining 'non-network' atoms have consistently been placed in the center of the triangles formed by network atoms. For this atom subset, no discrimination has been made between different atom types (equal diameter chosen). The Cu atom ordering has been highlighted with broad green lines, as in Fig. 1. The dashed red lines denote the C and Q' unit cells. (c) The four different overlapping local geometries, together fully comprising C and Q'. Geometry G1 (G4) incorporates all network (Cu) atoms. In three dimensions, the central non-network atom in geometry G2 (G3) will have five-fold (four-fold) coordination. Note that each network atom is always fully surrounded by non-network atoms, and vice versa

A brief consideration shows that both C and Q' as represented in Figs. 2a and 2b can be regarded as comprised entirely of the same four overlapping geometries G1 – G4, shown in Fig. 2c. All these geometries are constructed as possessing a central atom ('site') plus its immediate, projected environment. Allowing for undecided central atom

heights, G1 describes the state of all network atoms for the two phases. Each network atom is entirely surrounded by non-network atoms in this projected representation. The remaining geometries G2 – G4 have non-network atoms at their center, surrounded by three network atoms. Focusing here only on the relative heights of these atoms, four non-equivalent geometries are possible in principle. Only three of these are realized in C and Q': we do not encounter any geometries with all network atom heights different from the central non-network atom height. Notably, for defect-free C and Q'/Q particles, Cu occupies only the geometry G4 in Fig. 2c, as is evident from the Cu overlay in Figs. 2a and 2b. We label this site the 'Cu site' below. The connection between the local geometries and the Si network will be further clarified in Sec. 3.3.

The above discussion stressed only local geometries centered on an atom. Also 'empty' geometries, similar to both G2 and G3, but missing the central atom, exist in C and Q'/Q. For two reasons, omitting these geometries in Fig. 2c is presumed a safe option. Firstly, empty and filled geometries G2 and G3, respectively, (and vice versa) always alternate along the network *c*-axis for precipitates fully coherent with fcc Al along this direction. Secondly, the interatomic distances in empty geometries are always 4 Å or more, implying secondary importance to phase stabilization.

3.3. Hypothesis for a metastable phase construction principle

Compared to the deconstruction of C and Q'/Q into local geometries in Sec. 3.2, a similar attempt to unravel the degree of local ordering for the disordered L phase is arguably more challenging. In Sec. 3.1, we hypothesized from the HAADF-STEM images of Fig. 1 that all three phases may bear close structural resemblance. Recent experimental investigations of disordered phases in Al–Mg–Si–Ge–Cu [28], and in Al–

Mg–Si with Cu trace elements [27], add importantly to this suspicion. In [28], precipitates clearly resembling the L phase of Al–Mg–Si–Cu were fully deconstructed through a labeling of all atom heights. The analysis in that work highlighted strong levels of local ordering. This ordering can be readily extended, with the aid of Fig. 2c in this work, to a complete deconstruction into the local geometries G1 – G4. The emerging hypothesis is that L be fully described by the geometries of Fig. 2c. Potentially, this claim may be expanded to concern all Cu-bearing phases of (2).

Fig. 3a presents schematically the details of this Al–Mg–Si–Cu metastable phase construction hypothesis. At the outset, we require that some or all of the local geometries in Fig. 2c be coupled in a defect free manner to create the complete structure. It follows from the overlapping of adjacent network geometries G1 that all non-network atom heights are generally well defined. The heights of all Si network atoms, by contrast, remain undecided (gray) in the absence of a specific choice of precipitate structure. When e.g. the well-ordered C phase is selected, this set of heights 'collapses' onto the repetitive pattern displayed in Fig. 2a. However, the presence of such a repetitive pattern, and hence a unit cell, is not a necessity in Fig. 3a. It is unproblematic to create a structure with no unit cell, but with the same level of local ordering as C and Q'/Q. These considerations hint at a more precise understanding of the network substructure significance (compare with, e.g. [27]). In Sec. 1, it was stressed that the metastable phases in Al–Mg–Si(–Cu) are linked by the network. Fig. 3a however emphasizes that bulk C and Q' are formally (Fig. 2a, 2b) *distinguished* solely by the choice of network specific to these phases. The common link is now the local geometries of Fig. 2c.

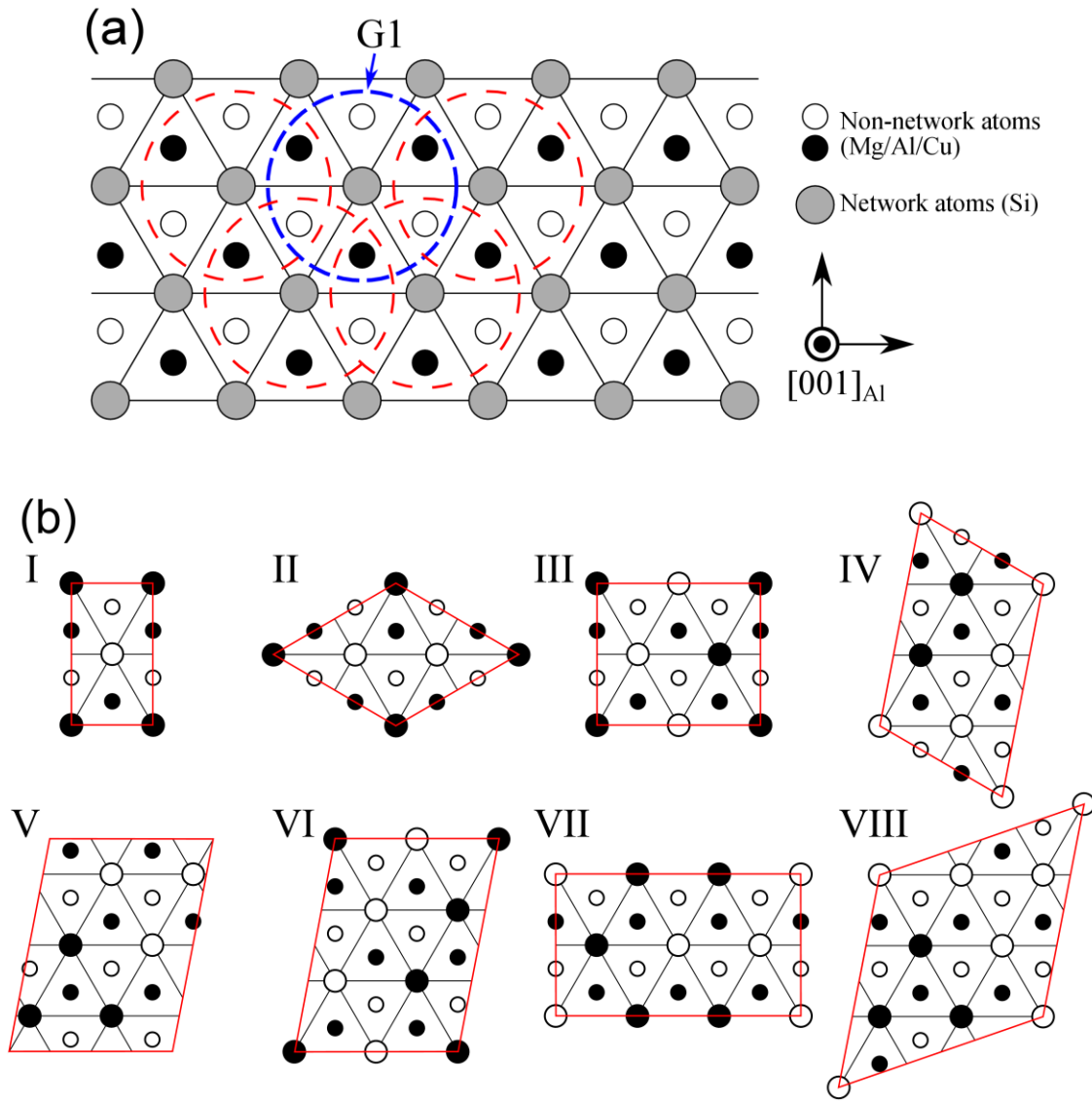


Fig. 3 Schematic representation and labeling of the selected set of allowed bulk phases constructed solely by the units of Fig. 2c. (a) Features of the generic structure with undefined Si network height distributions (nomenclature explained in Fig. 2).

Overlapping geometries G1, explaining this structure, have been shown. Note that not all combinations of network atom heights are compatible with the suggested construction principle. (b) Structures I – VII comprise the full set of periodic structures allowed by the construction principle, with up to six network atoms in the unit cell. Structures I, IV, VI and VII are hypothetical, *i.e.*, they have not been observed experimentally. Structures II, III and V resemble simplified β' [5], U2 [3] and the C

phase [7], respectively. Structure VIII, with 7 network atoms in the unit cell, resembles the Q'/Q phase [25]. This structure was added here due to its clear importance in L phase formation (Fig. 1c)

Computational studies of structures from Fig. 3a are only possible for the subset possessing a unit cell. In this work, we examine the stability of a representative set of such well-ordered structures (see Fig. 3b), each in their bulk state. Importantly, this set includes 'hypothetical phases'. These are structures not experimentally reported in isolation in the Al–Mg–Si(–Cu) system, but with bulk phase stabilizations formally embraced by the construction principle. The full set of structures is introduced in Sec. 5.1.

4. Computational details

The results presented in this work involve bulk precipitate structures only. Consider a Cu site free structure from Fig. 3b with a unit cell containing N network atoms, and hence a total number of $3N$ atoms. For this structure, we fully optimized selected configurations with composition $\text{Mg}_x\text{Al}_{2N-x}\text{Si}_N$. Here, x was varied from 0 to $2N$, with particular focus on the range around the calculated minimum formation energy (see below). The configurations were characterized by the network being fully occupied with Si, while on the non-network sites, only Al and Mg permutations were considered, with no Si present. These constraints were in accordance with conclusions from experimental observations, see Sec. 1. Additional calculations were carried out to test these basic assumptions: for selected configurations of each structure, we examined (i) introduction of Al on the network sites as well as (ii) Si introduction outside the network. None of these studies revealed any energetically preferred configurations. Mg

introduction on the network was deemed improbable. For the Cu containing phases, almost the same strategy was carried out. Cu atoms were introduced on the Cu site only (G4 in Fig. 2c), following the experimental conclusions of [8]. Based on earlier studies of the C phase [7], 100% Cu occupancy was always chosen on these sites. A numerical algorithm was developed and applied to generate the structures shown in Fig. 3b. This set comprised all structures up to the chosen upper limit on the value of N , see Sec. 5.1.

The driving force for precipitation for each precipitate structure ' P ' was estimated on the basis of the phase formation enthalpy ΔH_P^{SS} relative to constituent atoms in the solid solution (SS). Consider a Cu free structure $P\text{-Mg}_x\text{Al}_{2N-x}\text{Si}_N$, with the choice of atom ordering suppressed. Here, ΔH_P^{SS} , derived in units of eV/solute atom, is evaluated as:

$$\Delta H_P^{SS} = H(P\text{-Mg}_x\text{Al}_{2N-x}\text{Si}_N) - x\Delta H_{\text{Mg}}^{SS} - (2N - x)\Delta H_{\text{Al}}^{SS} - N\Delta H_{\text{Si}}^{SS}. \quad (3)$$

In this equation, $H(P\text{-Mg}_x\text{Al}_{2N-x}\text{Si}_N)$ denotes the cohesive energy of structure P . The quantity ΔH_X^{SS} refers to the formation enthalpy of a formally isolated substitutional element X in the fcc Al lattice (e.g., an alloying element in SS). This quantity was approximated as the cohesive energy difference between two 108 atom fcc supercells, one including X and one containing only Al, as:

$$\Delta H_X^{SS} = H(\text{fcc-Al}_{107}\text{X}) - (107/108)H(\text{fcc-Al}_{108}). \quad (4)$$

Extension to Cu site containing structures is straightforward. All calculations assumed a temperature of 0 K along with zero pressure, i.e., *formation energies* were determined.

Calculations were performed within the framework of DFT [29,30], employing Vanderbilt ultrasoft pseudopotentials [31] as implemented in the plane wave (PW) based Vienna *Ab initio* Simulation Package (VASP) [32,33]. For the description of the exchange-correlation functional, the Perdew-Wang generalized gradient approximation (GGA) [34] was used. A 234 eV PW cut-off was chosen in calculations. For all structures formally fully coherent with fcc Al along the network *c*-axis, the selected Monkhorst-Pack *k*-point grids included 22 *k*-points along the corresponding direction in reciprocal space. For the β' phase (Sec. 5.4), a compatible *k*-point density was selected.

5. Results and discussion

5.1. The set of candidate structures

Fig. 3b displays the sequence of well-ordered Al–Mg–Si(–Cu) structures selected for theoretical analysis. All structures were created using the construction principle outlined in Sec. 3. In particular, this implies that a complete deconstruction into the local geometries G1 – G4 of Fig. 2c is possible throughout. The sequence comprises all such structures with the number of network atoms in the unit cell $N \leq 6$. Computational simplicity is one reason for our focus on small unit cells. However, we also note that relatively few well-ordered metastable phases of (1) and (2) possess unit cells with $N \geq 7$. Apart from Q'/Q and the presumed isostructural B' phase [11], only β' [5] adds to this set. Further, a fair number of experimentally reported phases from both (1) and (2) are found to be closely connected with structures of Fig. 3b: Structures III ($N = 4$) and V ($N = 6$) are isostructural with U2–MgAlSi [3] and C–Mg₄AlSi_{3.3}Cu_{0.7} [7], respectively. Structure II ($N = 3$) closely approximates β' –Mg₉Si₅ [5], see Sec. 5.4. In contrast with β' , the B'/Q'/Q phase is not well approximated by any structure with $N \leq 6$. Given the clear importance of Q' to L phase stabilization (see Fig. 1c), this structure was

added (VIII) to the set in Fig. 3b. All remaining structures examined (I, IV, VI and VII) are hypothetical. In other words, they have not been experimentally reported, even in slightly modified versions, as pure phases in Al–Mg–Si(–Cu). We note that the C phase is the smallest Cu site containing, well-ordered phase obeying the proposed construction principle.

5.2. Calculated formation energies: support for the construction principle

Fig. 4a shows the calculated formation energies as a function of Mg content outside the network for the set of structures from Fig. 3b. For the Cu site free subset, i.e., the cells comprising only geometries G1 – G3 of Fig. 2c, the energies are noted to follow a common trend. Stabilization occurs at or near the MgAlSi composition (close-up in Fig. 4b), with comparatively shallow contours for higher Mg content. Energies and compositions for the minimum energy configurations are included in Table 1. Structure III, the only experimentally reported structure from the subset (U2 phase [3]) possesses the lowest energies among all Cu free structures at all compositions. At low Mg content, this structure is increasingly favored relative to Cu site free alternatives. However, the energies of the hypothetical structures are highly competitive. It is hardly clear from the results of Fig. 4 alone that only one of these phases is to be expected in an experimental investigation of the Al–Mg–Si alloy system. This conclusion provides a direct support for part of our hypothesis: the precise ordering of the geometries G1 – G3 of Fig. 2c matters only weakly to phase stabilization or chemistry. The result seems to underline another point indicated in Fig. 3a: the atomic interactions responsible for structure stabilization are metal-Si, and possibly metal-metal, but not Si-Si interactions. Structurally, on the other hand, the Si network *is* retained for each minimum energy configuration of Table 1. We stress that our bulk phase considerations leave out any

influence of precipitate-host lattice coherencies on phase formation. In other words, we have not shown at this stage that any of these phases *must* be expected to form – only that they are almost *equally likely* to do so, considering the energetic drive for formation.

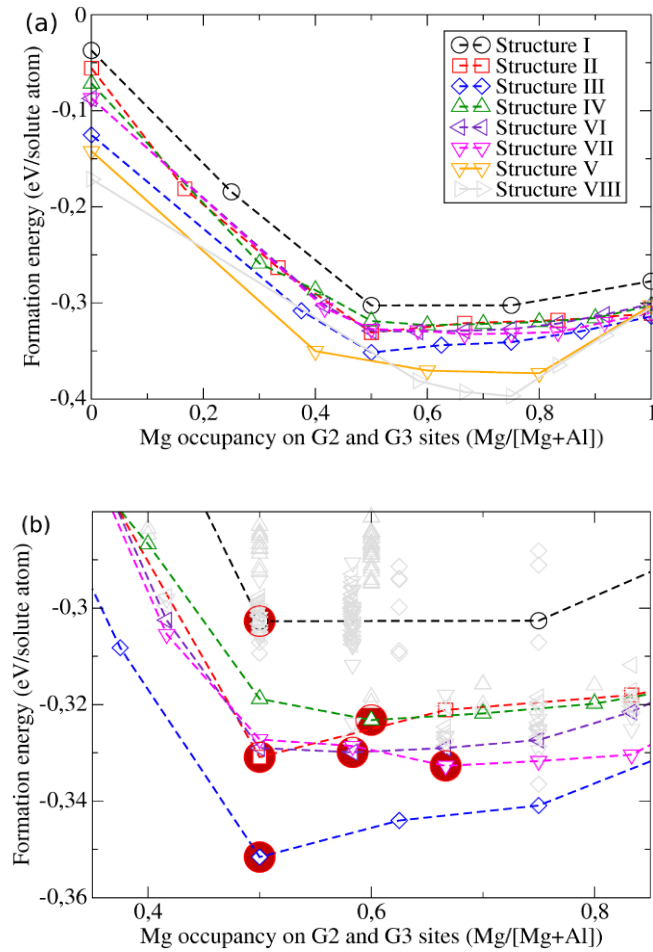


Fig. 4 Calculated formation energies for the set of structures from Fig. 3b, as a function of Mg content in the local geometries G2 and G3 of Fig. 2c. In these considerations, Mg is always replacing Al. In (a), the Cu bearing structures are distinguished by full lines connecting the points. (b) Enlargement of (a), including only the various Cu free structures and highlighting the energy minima by red circles. Here, also the full set of

structures examined for this subset has been highlighted (gray points)

Our studies involve only two Cu site bearing (geometry G4) structures. Both of these are experimentally reported phases in (2), see Sec. 5.1. Obviously, any conclusions on common trends in the energy variations within this 'set' are limited. As shown in Fig. 4a, the energies of these structures fall below the Cu free ones, with Q (Structure VIII) being more stable than C. This is expected from (2) as well as theoretical studies [7, 11]. Compared to [7], our C phase calculations adopted the same precision, but we evaluated the formation energies in units of eV/solute atom. This did not alter the predicted minimum energy composition, $\text{Mg}_4\text{AlSi}_3\text{Cu}$. For Q, our calculated minimum energy phase composition $\text{Mg}_9\text{Al}_3\text{Si}_7\text{Cu}_2$ also matched earlier work [11]. The composition for the metastable phases B', Q' is still under debate [6, 7, 11, 22]. As detailed studies into these issues were considered a case for future work, we entirely ignored B', discussing Q' only in the context of proposed coherency constraints, see Sec. 5.5.

Table 1: Minimized formation enthalpies and associated compositions for the structures of Fig. 3b. On optimization, all structural parameters were fully relaxed, with compositions for the Cu free phases assuming 100% Si occupancy on the network sites and no Si elsewhere. For the Cu bearing phases, Cu was confined to the Cu site (geometry G4 in Fig. 2c) following experimental observation [8]. Further, Si introduction on the non-network sites was considered following calculations for the C phase [7]

Str. label (Network at.)	Observed?	Cu site?	ΔH_p^{SS} (eV/solute at.)	Composition
I (2)	No	No	-0.3027	MgAlSi
II (3)	Almost ^a	No	-0.3309	MgAlSi
III (4)	Yes ^b	No	-0.3516	MgAlSi
IV (5)	No	No	-0.3232	Mg ₆ Al ₄ Si ₅
V (6)	Yes ^c	Yes	-0.3704	Mg ₄ AlSi ₃ Cu
VI (6)	No	No	-0.3299	Mg ₇ Al ₅ Si ₆
VII (6)	No	No	-0.3327	Mg ₄ Al ₂ Si ₃
VIII (7)	Yes ^d	Yes	-0.3970	Mg ₉ Al ₃ Si ₇ Cu ₂

^{a)} β' phase, composition Mg₉Si₅ [5]. See Sec. 5.4 for details.

^{b)} U2–MgAlSi [3].

^{c)} C–Mg₄AlSi_{3.3}Cu_{0.7} [7].

^{d)} Q'/Q phase (approximate composition Mg₉Al₃Si₇Cu₂) [3,25].

5.3. Deconstruction of an L precipitate

In Sec. 3.3, we proposed that the disordered L phase can be viewed as fully comprised of overlapping geometries G1 – G4 of Fig. 2c, following the pattern outlined for the well-ordered phases C and Q'/Q of the Al–Mg–Si–Cu system. In practice, this implies that each L precipitate should be represented by the structure in Fig. 3a with a specific choice of network substructure. The calculations described in Sec. 5.2 have paved the way for a justification of this hypothesis. Competitive formation energies have been highlighted for the majority of the Cu site free structures of Fig. 3b, allowing in principle for many of these structures to contribute locally to L. It remains to be

clarified, however, how the experimentally reported phase can actually be deconstructed.

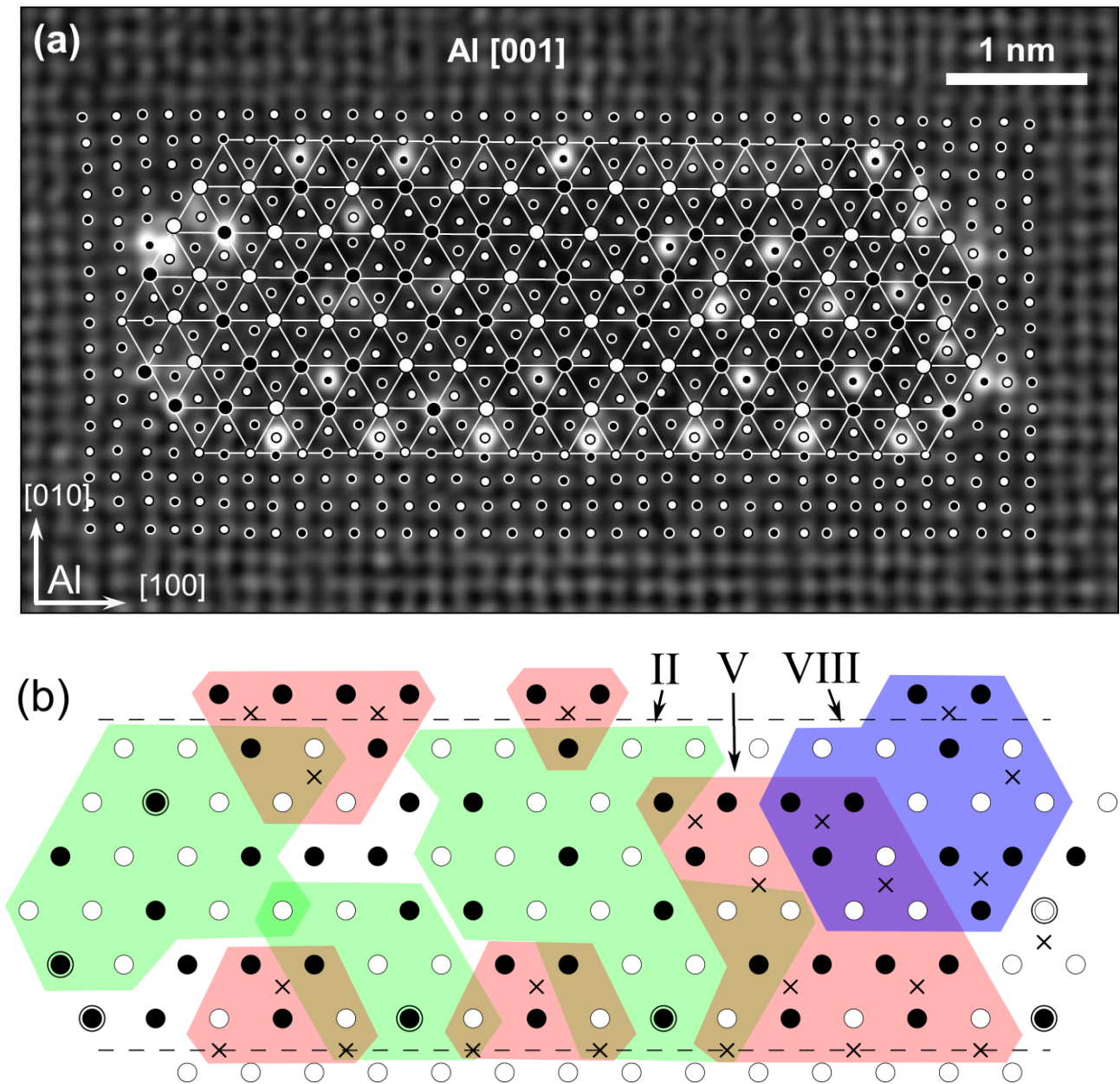


Fig. 5 (a) The L precipitate from Fig. 1c, with all atom heights (including those of adjacent host lattice columns) highlighted. Atoms within the precipitate are distinguished in a manner corresponding Figs. 2 and 3, with the network atom grid terminating at the approximate boundary to the host lattice. For the host lattice atoms, the non-network atom nomenclature has been used. (b) Schematic illustration of the

same precipitate. The Si network substructure and the Cu sites (local geometry G4 of Fig. 2c) have been highlighted with circles and crosses, respectively. Some precipitate boundary atoms from (a) have been excluded. A division into extended regions of structures from Fig. 3b has been stressed with colored areas: Structure II (green), V (red) and VIII (blue). Cu is observed (see (a)) to occupy a low number of Si network sites in the Cu site free Structure II. These sites are highlighted in (b) with larger, double-line circles

To probe this issue, we performed a structural analysis of the L precipitate of Fig. 1c. In Fig. 5a, the relative heights for the atoms needed to identify the underlying network substructure have been labeled. The procedure used here rests on the assumption that all precipitate atoms for the horizontal interfaces in the figure are located essentially on Al host lattice sites. The construction can then be completed exclusively from the observed movement of each non-network atom away from a network triangle center. This information is sufficient to distinguish the (relaxed) geometries G2 – G4 in Fig. 2c. Knowledge of the atom types is not required.

We find that this L precipitate is fully comprised of the overlapping local geometries of Fig. 2c. Fig. 5b displays a deconstruction of the precipitate into extended regions of well-ordered structures from Fig. 3b. Evidently, three different structures are dominating, namely the Cu site free Structure II and the Cu site containing Structures V (C) and VIII (Q'/Q). Mostly, but not always, individual extended regions overlap nicely, indicating smooth structural transitions.

Structure II bears close similarities with the β' phase (see Sec. 5.4), but has a different

orientation in the host lattice in Fig. 5b, relative to pure β' [5]. As discussed in Sec. 3.1, the same applies to Q' in L versus pure Q'. Judged from Fig. 5, both structures possess seemingly coherent interfaces with fcc Al along $\langle 100 \rangle_{\text{Al}}$. Even though none of the interface regions are highly extended in the cross-section plane, it is a question of general interest to address the level of coherency further. Comparing Figs. 3b and 5b for Structure II, we find that this phase possesses a row of atoms at alternating heights at the ultimate interface location, structurally matching the fcc Al boundary. In Fig. 3b, this line is horizontal, and connecting non-network atoms only. In the absence of experimental data on Structure II, we turn to studies of β' [5]. From here, 'agreeable' ($\approx 2\%$) misfit values along the interface are suggested. In addition, studies of β' in Al–Mg–Ge [35] provide direct experimental support for the discussed phase reorientation being energetically competitive. For Q', the structural conditions for a coherent interface appear satisfied as well, through a horizontal line connecting non-network atoms only in Fig. 2b. We stress that this figure should be reoriented for the consideration, with $[510]_{\text{Al}}$ replaced by $[100]_{\text{Al}}$. However, on approximating the Q' dimensions with experimentally reported Q values [11], prohibitive misfit values ($\approx 25\%$) are predicted. While not at odds with the observations in Fig. 5, this conclusion strongly suggests that *only local* Q' regions are allowed in L.

As a result of the Q' and Structure II reorientations for the L precipitate examined, the Si network orientation is *effectively locked* by the C part. This in turn indicates that the precipitate nucleus is located around a C domain. In support of this hypothesis, Q' is gaining dominance [8] upon overaging in (2). This suggests a higher barrier to pure Q' phase formation, compared to C. We further note that, even if L starts as small C nuclei, growth of Cu-poor regions within the L structure may still be triggered whenever Cu is

not present in the vicinity. The experimentally reported [36] Cu diffusivity in Al is comparatively low. Presumably, this makes Cu the rate limiting factor to the growth of a well-ordered Cu containing phase, in turn triggering disorder. As indicated in the previous paragraph, the Cu free L domains formed should bear a close structural coupling to *both* the existing Cu containing 'nucleus' as well as fcc Al, at least on a scale comparable to the domain unit cells. This nucleation and growth scenario differs fundamentally from the situation in Al–Mg–Si, with presumed influence both on the ultimate domain orientations and the selection of 'realistic' L constituents from Fig. 3b.

As noted in Sec. 3.1, Cu in L is not completely confined to the Cu site, but most prominently incorporated in certain isolated network columns away from the C and Q' local regions for the precipitate in Fig. 5a. The deconstruction in Fig. 5b reveals that these Cu atoms consistently occupy *the same site* in Structure II, indicating that the Cu incorporation here is strongly preferential. This tendency was discussed recently by Saito *et al.* [27], in experimental work on metastable phases in Al–Mg–Si alloy systems with weak Cu additions.

5.4. Proposed links between the local geometries and selected Al–Mg–Si phases

Taking into account the presently available amount of experimental knowledge on the Al–Mg–Si–Cu alloy system, the considerations of Sec. 5.2, 5.3 have made a strong case for all Cu containing phases in (2) being fully comprised of the local geometries of Fig. 2c. An intriguing question (see Sec. 1) is the relevance of these considerations to the Al–Mg–Si precipitation sequence. Most of the structures examined in Fig. 4 are Cu free, and thus represent hypothetical or real structures in Al–Mg–Si as well (see Sec. 5.1). For this set, trends in the formation energy dependence on

composition can be readily discussed. In the following, we stress a series of potential links between these structures and known phases in Al–Mg–Si. These considerations are primarily meant as a motivation for future studies. In particular, we note that only some of the metastable phases in (1) come under the category of structures highlighted in Fig. 3a. For other theoretical discussions on Al–Mg–Si metastable phase links, see [12, 13].

The formation energies in Fig. 4a were computed within the assumption of a high solute atom diffusivity in the precipitates, see, e.g. [37]. Locally, however, *Mg always replaces Al at a clear energy gain* on the non-network sites according to our calculations. The reason why Al is ultimately present on roughly half of these sites in Fig. 4b is related to the difference between the energy gains upon Mg introduction in the two geometries G2 and G3 of Fig. 2c. Of these two sites, Mg generally prefers G2. The largest difference in the two replacement energies is encountered for structure III; ≈ 0.58 eV/atom (G2) versus ≈ 0.24 eV/atom (G3). The non-network sites for the Cu site free structures in Fig. 4 are always evenly shared between G2 and G3. Hence, a minimum formation energy (evaluated in units of eV/solute atom) around the MgAlSi composition is to be expected. When no constraints on the Mg/Si ratio are present in the calculations, and diffusion on the non-network sites is formally unrestricted, any Mg atom occupying a G3 site can technically speaking always find a nearby G2 site providing higher stabilization. We stress that, for the physical system, this view may apply for some [3], but not necessarily all precipitates. The crucial points are the solute atom diffusivity assumption, and, potentially, the presence of interface growth obstacles [37]. Note that the larger fraction of G2 geometries for the Cu containing structures of Fig. 3b partly explains why these structures are stabilized at higher Mg content (Fig. 4a).

In the context of a link between the local geometries of Fig. 2c and the Al–Mg–Si alloy precipitates, the β' phase is of particular interest. Formally, one may obtain β' from Structure II [5] by decreasing the atom separation along one of the three network chains in the unit cell of Fig. 3b. This process has been described schematically in Figs. 6a and 6b. Unlike Structure II, however, β' is not stabilized at $\text{Mg}/\text{Si} \approx 1$ according to experiment. Rather, it was reported [5] to be Al-free. For a justifiable link between these two structures to be established, one would have to elucidate this compositional difference by way of energy considerations. The task here would be to show that Structure II may effectively be a precursor of β' .

To probe this issue, the following calculations were carried out. Consider the lowest energy configurations for Structure II in the composition range $0.5 \leq \text{Mg}/(\text{Mg}+\text{Al}) \leq 1$ of Fig. 4a. For each of these configurations, we introduced the network substructure change described in Fig. 6b. We then optimized the resulting β' configurations for comparison of the energies. As shown in Fig. 6c, β' is found to be more stable than Structure II at the Al-free compositions, as expected. Our calculated energies here closely match those in [5]. Also, the β' minimum formation energy is below the Structure II counterpart, reflecting the experimental observation of the former isolated phase only. However, at the point of Structure II minimum formation energy, $\text{Mg}/(\text{Mg}+\text{Al}) = 0.5$, β' is decidedly *less stable*. An energetic drive for a $\text{II} \rightarrow \beta'$ transition is established only above $\text{Mg}/(\text{Mg}+\text{Al}) \approx 0.9$. Two important results are indicated here. Firstly, β' may indeed grow as Structure II in the early stages. Secondly, Mg-rich Structure II configurations may be achievable.

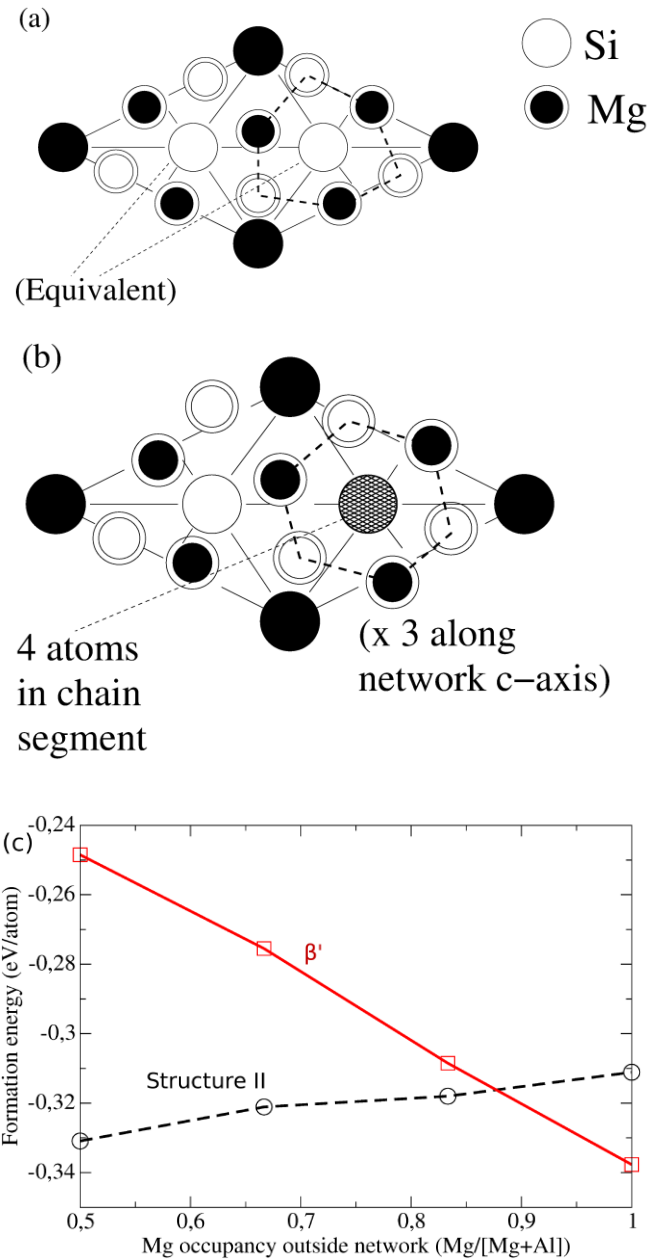


Fig. 6 (a) Schematic representation of a (hypothetical) Structure II-Mg₂Si, in the same orientation as in Fig. 3b. (b) The β'-Mg₉Si₅ phase, viewed in the same projection as (a). Compared to [5], the β' unit cell has been shifted to move the corner atoms (gray) to the cell interior. In contrast with Structure II, the β' Si network comprises chains with different average atom separation. This network modification is slightly changing the symmetry of projected atomic columns in the precipitate cross-section plane. Further, it triples the cell dimension along the network *c*-axis (precipitate main growth direction).

(c) Calculated formation energies for Structure II and β' as a function of Mg content on the non-network sites. The β' phase is stabilized only very near the experimentally reported Al-free structure according to these studies

Our theoretical considerations find potential experimental support in the reported β' /Al interface characteristics for both Al–Mg–Si [38] and Al–Mg–Ge [35]. Both studies stressed clear signs of a 'shell' isostructural to Structure II at the interface boundary. In the vicinity of the seemingly fairly diffuse [38] interface, the precipitate is likely less solute-rich. The experimental observations may hence be interpreted as a sign of a *stabilization* of Structure II over β' in this region, as predicted in Fig. 6c. In turn, this supports our hypothesis that the earliest β' precipitates are fully isostructural to Structure II.

If the indicated “local desire” for Mg_2Si compositions among the Cu site free structures of Fig. 3b were connected with a phase stabilization principle, one would expect some clear link between this principle and the Al–Mg–Si equilibrium phase β - Mg_2Si [39] in (1). As discussed in Sec. 1, β does not host the Si network. However, as shown in Fig. 7, this structure can be fully deconstructed into local geometries from the full set discussed in Sec. 3. We stress that this intriguing structural result must ultimately be accompanied by total energy calculations. In this process, one must move beyond the network constraint of Fig. 3a, in order to clarify if β can also be regarded as *chemically* deconstructed into local geometries.

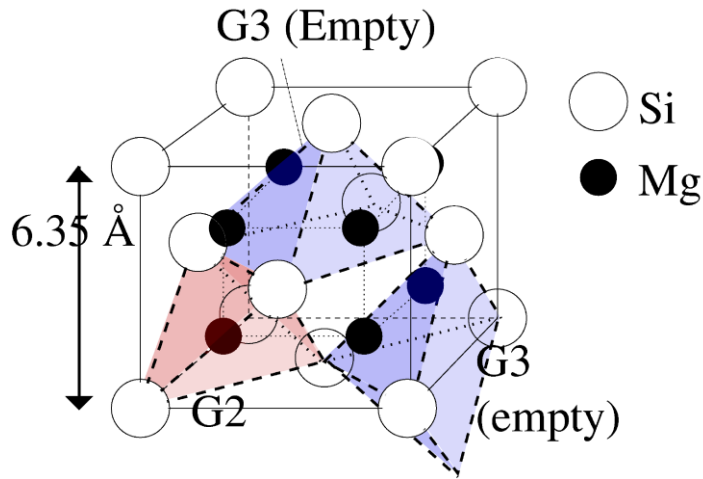


Fig 7 Schematic illustration highlighting the full deconstruction of the Al–Mg–Si equilibrium phase β -Mg₂Si into local geometries from the set discussed in Sec. 3. The anti-fluorite β phase unit cell shown can be viewed structurally as comprised by sixteen non-overlapping geometries: eight local geometries of type G2 (each Mg atom resides in a tetrahedral interstitial of the Si fcc substructure), and eight 'empty' local geometries of type G3 (pairwise enclosing the octahedral interstitials)

5.5. Influence of precipitate-host lattice coherencies

When analyzing the deconstructed L precipitate of Fig. 5 in Sec. 5.3, we stressed how the precipitate-host lattice coherencies may ultimately leave only certain structures from the set in Fig. 3b as acceptable constituents of L. This consideration was related to the general expectation that a maximum level of *structural* overlap at the interface between a fully defined precipitate and host lattice will reduce the barrier to nucleation of that given precipitate. Recently, Torsæter *et al.* [7] proposed an additional influence of precipitate-host lattice coherencies, with consequences to the *precipitate chemistry*. Through combined theoretical and experimental studies of the C phase, the authors showed that the experimentally reported C phase composition Mg₄AlSi_{3.3}Cu_{0.7}

correlated with the elimination of the precipitate-host lattice misfit along the precipitate main growth direction. It was argued that this correlation could represent a fundamental aspect of precipitate growth. The metastable phases may generally evolve according to a *simultaneous* minimization of formation energy and main growth axis misfit, as opposed to formation energy minimization only.

In the present work, we have examined the correlation between compositions and combined misfit/formation energy minimization for selected structures of Fig. 3b, following the procedure of [7]. Since experimental comparison is of key interest here, we limited our studies to observed structures and proposed metastable phase precursors. For Structure III at the MgAlSi composition, we find a bulk cell dimension of 4.048 Å along the network *c*-axis, with clearly growing misfits for more Mg-rich configurations. In other words, a seemingly close agreement is encountered with experimentally reported U2–MgAlSi, *regardless* of the level of solute atom diffusion within the precipitate (see Sec. 5.4). For Structure II, a composition close to Mg₅AlSi₃ is predicted. Interestingly, this is very close to the point where a drive for a transition to β' was proposed in Fig. 6c. For the C phase, mixing of Al/Si onto the Cu sites was argued in [7] to produce the lowest energy configurations with negligible main growth axis misfit. Our results differ little from those conclusions, though Al replacement of Cu is now favored over Si. For Q', taking into account the low Cu atom diffusivity stressed in Sec. 5.3, the most probable configuration involves ≈ 30% Cu exclusion from the Cu sites, compared to Q. This value is in fair agreement with the experimentally reported [7] ≈ 50% Cu reduction.

6. Conclusions

In this work, we have shown that the well-ordered metastable phases C and Q' of the Al–Mg–Si–Cu system are constructed by an identical set of overlapping local metal–Si geometries. Employing experimentally established similarities among the well-ordered and disordered metastable phases in Al–Mg–Si–Cu, we have proposed that the same set of local geometries can be used as well to fully explain the latter set of structures. We have obtained theoretically the formation energies and compositions for a representative set of Cu site free structures, all obeying the proposed construction principle. In support of our disordered phase hypothesis, these quantities were found to be practically insensitive to the ordering of the local geometries. The set of structures examined includes some experimentally reported phases in Al–Mg–Si: U2, B' (presumed fully described) and β' (closely approximated). By comparison, the influence of the Cu-bearing local geometry on the proposed principle is less clear, with calculations probing only the two experimentally reported Al–Mg–Si–Cu well-ordered metastable phases C and Q'. Structural analysis of a selected L precipitate showed that an almost full deconstruction into well-ordered regions of only three structures could be made: away from the local regions of C and Q', directly visible in experiment, a local geometry ordering leading to Structure II largely prevailed. Both Structure II and Q' are noted to be reoriented relative to their isolated state (the closely connected β' in the former case). We hypothesize from this observation that L nucleates as C, with formation of Cu free domains initiated when the slowly diffusing Cu is not available. The domain reorientations in L presumably stress the importance of retaining coherencies with both C and fcc Al for this precipitate. For the set of Cu site free structures examined, we note that Mg always replaces Al favorably *locally* in our calculations. Since the Al–Mg–Si equilibrium phase β -Mg₂Si can be deconstructed into local geometries, we hypothesize that the construction principle for the Cu site free

structures is linked to a desire for Mg₂Si compositions. Preliminary support for this hypothesis from energetic considerations has been discussed. In particular, a II → β' structural transition upon growth of the isolated Al–Mg–Si precipitate has been proposed.

Acknowledgments

This work has been financially supported by the Research Council of Norway via the MultiModAl project (project no. 205353), the FRINATEK researcher project (NRC ES494770), and the “Smart 6xxx Alloy Development for Rolling and Extrusion” project (NRC ES474768). For the last project, financial support from Hydro Al Research and Technology Development is also acknowledged. Simulations were performed through access to the NOTUR facilities. Flemming Ehlers gratefully acknowledges enlightening discussions with Dr. Ruben Bjørge of SINTEF.

References

- [1] Zandbergen HW, Andersen SJ, Jansen J. *Science* 1997;277;1221.
- [2] Hasting HS, Frøseth AG, Andersen SJ, Vissers R, Walmsley JC, Marioara CD, Danoix F, Lefebvre W, Holmestad R. *J Appl Phys* 2009;106;123527.
- [3] Andersen SJ, Marioara CD, Frøseth A, Vissers R, Zandbergen HW. *Mater Sci Eng A* 2005;390;127.
- [4] Andersen SJ, Marioara CD, Vissers R, Frøseth A, Zandbergen HW. *Mater Sci Eng A* 2007;444;157.
- [5] Vissers R, van Huis MA, Jansen J, Zandbergen HW, Marioara CD, Andersen SJ. *Acta Mater* 2007;55;3815.

- [6] Vissers R, Marioara CD, Andersen SJ, Holmestad R. *Aluminium Alloys* 2008;1263.
- [7] Torsæter M, Ehlers FJH, Marioara CD, Andersen SJ, Holmestad R. *Philos Mag* 2012;92;3833.
- [8] Marioara CD, Andersen SJ, Stene TN, Hasting H, Walmsley J, van Helvoort ATJ, Holmestad R. *Philos Mag* 2007;87;3385.
- [9] Marioara CD, Andersen SJ, Zandbergen HW, Holmestad R. *Met Mater Trans A* 2005;36A;691.
- [10] Edwards GA, Stiller K, Dunlop GL, Couper MJ. *Mater Sci Forum* 1996;217-222;713.
- [11] Ravi C, Wolverton C. *Acta Mater* 2004;52;4213.
- [12] van Huis MA, Chen JH, Zandbergen HW, Sluiter MHF. *Acta Mater* 2006;54;2945.
- [13] van Huis MA, Chen JH, Sluiter MHF, Zandbergen HW. *Acta Mater* 2007;55;2183.
- [14] van Huis MA, Sluiter MHF, Chen JH, Zandbergen HW. *Phys Rev B* 2007;76;174113.
- [15] Starink MJ, Cao LF, Rometsch PA. *Acta Mater* 2012;60;4194.
- [16] Chen JH, Costan E, van Huis MA, Xu Q, Zandbergen HW. *Science* 2006;312;416.
- [17] Cayron C, Sagalowicz L, Beffort O, Buffat PA. *Philos Mag A* 1999;79;2833.
- [18] Andersen SJ, Marioara CD, Vissers R, Frøseth A, Derlet P. *Proceedings 13th European Microscopy Congress (EMC 2004);Vol. 2;599.*
- [19] Andersen SJ, Marioara CD, Vissers R, Torsæter M, Bjørge R, Ehlers FJH, Holmestad R. *Mater Sci Forum* 2010;638-642;390.
- [20] Zhang WZ, Yang XP. *J Mater Sci* 2011;46;4135.
- [21] Marioara CD, Andersen SJ, Boothroyd CB, Holmestad R. *Aluminium Alloys* ISBN 978-4-905829-11-9 2010;424.
- [22] Wolverton C. *Acta Mater* 2001;49;3129.

- [23] Ehlers FJH, Wenner S, Andersen SJ, Marioara CD, Holmestad R. ICAA13: 13th International Conference on Aluminium Alloys (software) ISBN: 978-1-1184-5804-4 2012;279.
- [24] Chakrabarti DJ, Laughlin DE. *Prog Mater Sci* 2004;49;389.
- [25] Arnberg L, Aurivillius B, *Acta Chem Scand A* 1980;34;1.
- [26] Nellist PD, Pennycook SJ. *Ultramicroscopy* 1999;78;111.
- [27] Saito T, Marioara CD, Andersen SJ, Lefebvre W, Holmestad R. *Philos Mag* 2013; DOI:10.1080/14786435.2013.857051.
- [28] Bjørge R, Andersen SJ, Marioara CD, Etheridge J, Holmestad R. *Philos Mag* 2012;92;3983.
- [29] Hohenberg P, Kohn W. *Phys Rev* 1964;136;B864.
- [30] Kohn W, Sham LJ. *Phys Rev* 1965;140;A1133.
- [31] Vanderbilt D. *Phys. Rev B* 1985;32;8412.
- [32] Kresse G, Hafner J. *Phys Rev B* 1993;47;R558.
- [33] Kresse G, Furthmüller J. *Comput Mater Sci* 1996;6;15.
- [34] Perdew JP, Chevary JA, Vosko SH, Jackson KA, Pederson MR, Singh DJ, Fiolhais C. *Phys Rev B* 1992;46;6671.
- [35] Bjørge R, Dwyer C, Weyland M, Nakashima PNH, Marioara CD, Andersen SJ, Etheridge J, Holmestad R. *Acta Mater* 2012;60;3239.
- [36] Du Y, Chang YA, Huang B, Gong W, Jin Z, Xu H, Yuan Z, Liu Y, He Y, Xie FY. *Mater Sci Eng A* 2003;363;140.
- [37] Ehlers FJH. *Comput Mater Sci* 2014;81;617.
- [38] Teichmann K, Marioara CD, Andersen SJ, Marthinsen K. *Mater Char* 2013;75;1.
- [39] Baranek P, Schamps J, Noiret I. *J Phys Chem B* 1997;101;9147.